International Symposium
On Turbulence and Shear Flow
Phenomena (TSFP-9)
June 30 - July 3, 2015 *Melbourne, Australia*

HYPERSONIC BOUNDARY LAYER TRANSITION INDUCED BY DIFFERENT ISOLATED ROUGHNESS ELEMENTS

Zhiwei Duan
School of Aerospace Engineering
Tsinghua University
Beijing, P.R. China, 100084
dzw15@tsinghua.edu.cn

Zhixiang Xiao
School of Aerospace Engineering
Tsinghua University
Beijing, P.R. China, 100084
xiaotigerzhx@ tsinghua.edu.cn

ABSTRACT

Hypersonic boundary layer transition from laminar to turbulent induced by different isolated roughness elements, are investigated using direct numerical simulation based on finite volume formulation with the MDCD scheme. The effect of roughness shape (ramp, diamond and cylinder) on transition mechanisms, aerodynamic and aerothermodynamics performance is studied. It is found that that the transition is dominated by the instability of the three-dimensional shear layer. The stream-wise transition location is almost the same for these three roughness elements, while the width of turbulent wake, the increasement of drag force and heat flux for the cylindrical roughness are largest, compared with the other two shapes.

INTRODUCTION

Roughness induced boundary layer transition plays an important role in the aerodynamic and thermodynamic design of hypersonic vehicles, as roughness will lead to an earlier transition than the smooth surface condition. The turbulent boundary layer results in higher heat transfer rate as well as the skin friction than laminar one, which will cause the excessive design of thermal protection systems for hypersonic vehicles. On the other hand, turbulent flow can help to eliminate the boundary layer separation on the forbody of scramjet vehicles, such as X-43A and X-51A, as well as to enhance the mixture of the fuel and air in the engine.

There are many factors that influence the effect of roughness on transition, such as the geometry of roughness (including height, width, shape and the space between two roughness elements), boundary layer thickness, Reynolds number, Mach number and wall temperature, etc. (Schneider, 2008) .

Among the geometrical factors, the roughness height plays the most important role. Van Driest and Blumer (1962) found that when the roughness is shorter than the "critical height", it will have no effect on the boundary layer transition; another important concept is the "effective height", which means that, the boundary layer can be triggered to turbulence effectively as long as the roughness exceeds this height.

The ideal roughness element trips the flow to turbulence very rapidly, without producing much drag at the roughness itself and encountering severe thermal environment. Whitehead (1969) found a vortex-generating fin had less drag for the same frontal area, suggesting it might improve on the usual spheres for tripping purposes. Berry et al. (2001) compared five different boundary-layer trip devices on the 33.3%-scale forebody model of Hyper-X in three hypersonic wind tunnels, a ramp-type (Trip 2C) was finally selected, based on a minimization of entrained vortices within the turbulent region and consideration of the thermal survivability of the trip.

Sterrett et al. (1967) found that the shape of the tripping element is not too important in producing transition at hypersonic speeds, as long as an appreciable part of the frontal area of the element is located near the top of the element. Tirtey (2008) found that the flow fields around the three-dimensional roughness showed strong similarities with the generation of various number of streamwise vortices, however the influence of the number of vortices on the roughness efficiency to promote transition was not clear.

Choudhari et al. (2010) performed the parametric study of flow past an isolated roughness element in a Mach 3.5 laminar flat plate boundary layer. For the diamond, cylinder and spherical roughness, it was found that the streak amplitudes for the diamond trip and cylindrical trips are comparable to each other, while the spherical trip leads to lower streak amplitudes, which means the perturbation by the spherical trip was weaker than the other two trips. Van den Dynde and Sandham (2014) investigated the effect of roughness element shape (smooth bump, flat top and ramp), platform (cylindrical, square and diamond) on transition mechanisms using direct numerical simulation, they found that the roughness element platform has a marginal effect on instability growth and transition, while the frontal profile shape has a large effect.

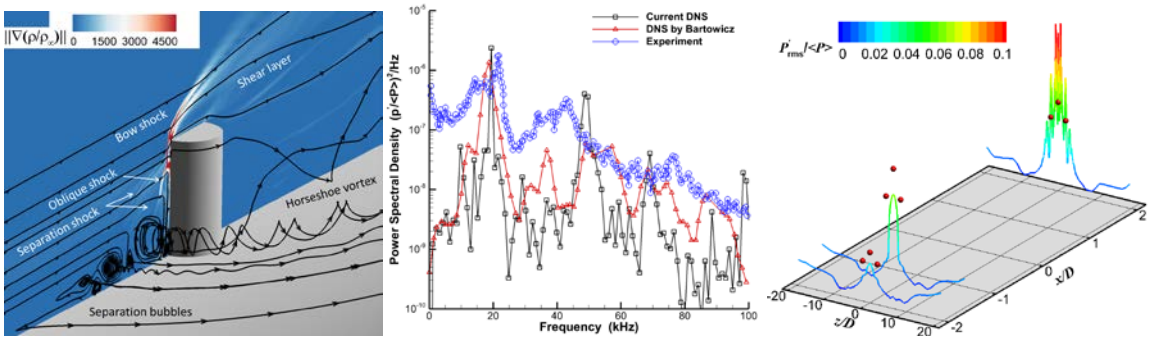

(a) (b) (c)

Figure 1. Flow around the cylindrical roughness in the Boeing/AFOSR quiet wind tunnel
(a) Flow topology, (b) Flow fluctuations 1D before the cylinder, and (c) $p'_{rms}/<P>$ near the cylinder

NUMERICAL STRATEGRY

The in-house code, UNITs (Unsteady NavIer-sTokes equation solver), based on a cell-centered finite volume formulation with multi-block structured grids, is mainly developed to accurately resolve the unsteady flows. The inviscid fluxes are solved using rotated Roe Riemann solver, through 4th order MDCD-WENO reconstruction for the original variables (Wang et al. 2012). A modified fully implicit lower-upper symmetric Gauss-Seidel (LU-SGS) with Newton-like sub-iterations in pseudo time is taken as the time marching method when solving the Navier-Stokes (N-S) equations.

Code Validation

The validation and some application of the MDCD-WENO scheme were performed in the authors' previous paper (Duan et al. 2014), where it shows good performance in simulating compressible unsteady flows for RIT problem. Our simulation is about the cylindrical roughness induced hypersonic boundary layer transition, the experiment is conducted by Wheaton et al. (2013) in the Boeing/AFOSR Mach-6 Quiet Tunnel in Purdue University.

Due to the 'junction flow' of the cylinder and wind tunnel, three pairs of separation bubbles are formed upstream of the roughness, travelling with the main flow to form horseshoe vortices. In the hypersonic flow, multiple shock waves induced by the separation bubbles and the roughness can also be observed, as shown in Figure 1(a).

The pressure fluctuation at the location of 1D before the roughness element on the symmetric plane is recorded, both the dominated frequency and amplitude of power spectral density of normalize pressure (p'/<P>) agrees well with the experiment and DNS result of Bartkowicz (2012), as shown in Fig. 2(a). The dominated frequency in our simulation is about 19.2 kHz, while it is about 21 and 18 kHz in the experiment and Bartkowicz's simulation.

The root mean square of the normalized pressure (p'rms/<P>) near the cylinder shows good agreement with the experiment, as shown in Fig. 2(b), in which the red points are the experimental results.

Computational Setup

The model is a roughness element placed on a flat plate, which is similar with the experiment performed by Tirtey (2008). The geometrical parameters of these roughness elements are shown in Figure 2 and Table 1.

The freestream Mach number is 6, the unit Reynolds numbers are 9.2×10^6, 1.8×10^7 and 2.6×10^7/m, respectively. In the numerical simulation, the highest Reynolds number condition is chosen; the freestream temperature T_∞ is set to be 70K, and the wall temperature T_w is set to be 300K, as shown in Table 2. These flow parameters are similar with the experiment. The undisturbed boundary layer thickness at the roughness location (δ) is approximately 0.79mm, the roughness Reynolds number ($Re_h = \rho_h U_h h/\mu_h$) is about 1.6×10^4.

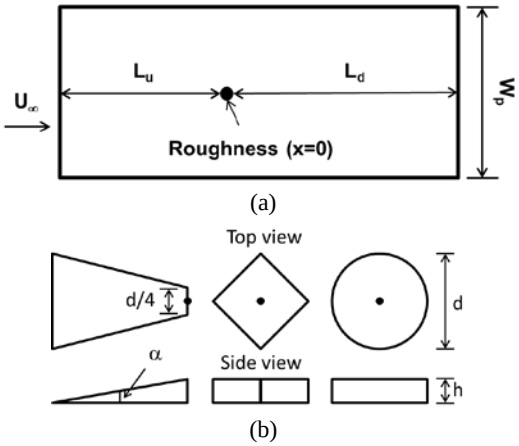

(a)

(b)

Figure 2. Sketch of the the roughness elements

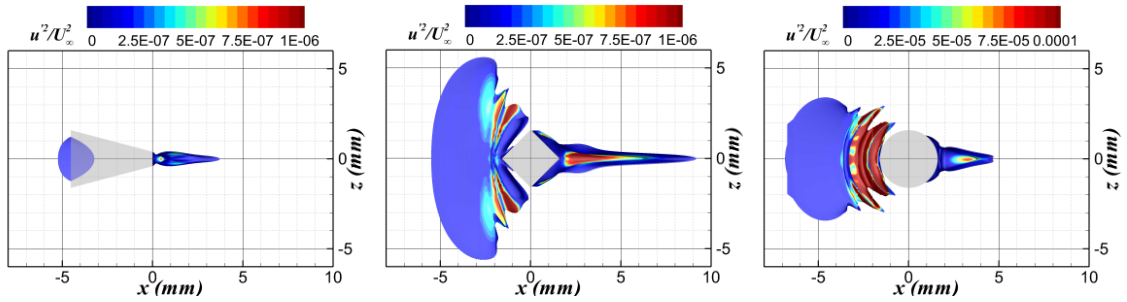

Figure 3 Separations flows around the roughness elements

Table 1. Geometry of the roughness elements

L_u	L_d	W_p	h	d	α
60mm	100mm	34.1mm	0.8mm	3.2mm	10^0

Table 2. Flow parameters

Ma_∞	T_∞(K)	T_w(K)	δ(mm)	Re_h
6	70	300	0.79	1.6×10^4

RESULTS AND DISCUSSIONS

Flow-field Around Roughness Elements

The separation flows around these roughness elements are illustrated by the iso-surface of negative streamwise velocity ($-1\times10^{-4}\ U_\infty$), which is colored by the Reynolds stress *u'u'*, as shown in Figure 3.

For the ramp roughness, the upstream separation flow is restricted in a relatively small zone, about 1.98mm long and 2.32mm wide. The small velocity fluctuation on the separation flow surface indicates the separation bubble may be steady here. Downstream of the ramp, the separation zone is about 3.72mm long, and shows higher level velocity fluctuation.

The separation flow around the diamond extends about 3.91 upstream and 11.22mm in the spanwise (*z* axis) direction. The flow fluctuation is small near the symmetric plane, while its magnitude gradually increases away from the symmetric plane. The downstream separation bubble is about 7.6mm long, and its fluctuation is at a higher level than upstream separation flow.

For the cylinder roughness, the upstream separation bubble is the longest among these roughness elements (about 5.25mm), and is 6.85mm wide. The separation flow shows a high level fluctuation, about two magnitudes higher than the ramp and diamond roughness. The downstream separation zone is the shortest, about 3.02mm in the streamwise direction.

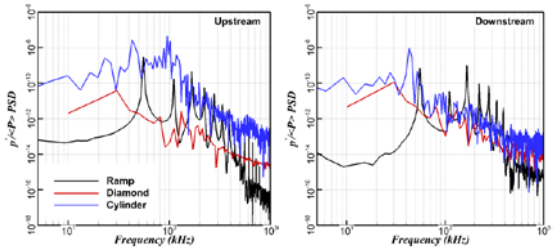

Figure 4. Normalized pressure fluctuation upstream and downstream of the roughness elements

The unsteady flow fluctuations on the flat plate below the separation zone are recorded, as shown in Figure 4. For the ramp roughness, the upstream sample point is located at x=-4.5 and y=z=0mm, the downstream sample point is located at x =2.3 and y=z=0mm. For the diamond and cylinder, the upstream and downstream sample points are at x=-2.4 and 3.4mm, respectively.

The upstream and down separation flows show periodic motion, the dominated frequencies are about 55.27, 30.19 and 42.58 kHz for the ramp, diamond and cylinder, respectively. For the ramp roughness, the unsteady flow exhibits several distinguished harmonic frequencies, such as 110.54, 165.82, 221.09 kHz, and so on. But for the square and cylinder, the harmonic frequencies are not as obvious as the ramp one. The fluctuation energy concentrates near the low frequency region; the magnitude of fluctuation energy for the ramp is the smallest, while it's the largest for the cylinder.

As shown in Figure 5, the roughness element in the hypersonic boundary layer will form a strong 'bow shock' before it, also a series of separation shocks exhibit due to the separation bubbles. Downstream of the roughness element, expansion wave and reattach shock wave are formed. In Figure 5, the three-dimensional shock systems are illustrated using the 'normal Mach number', the iso-surface of Ma_n=1 stands for the shock wave, which is defined as equation (1).

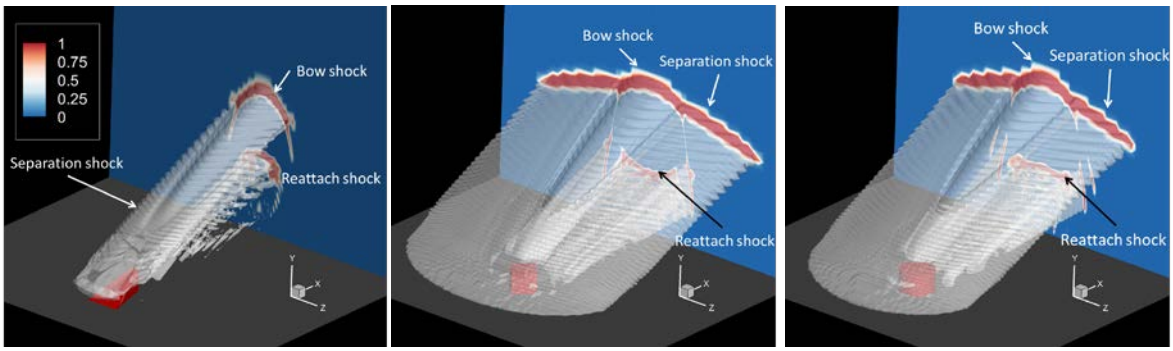

Figure 5. Shock wave systems around the roughness elements

$$Ma_n = \frac{\overrightarrow{Ma}\cdot\nabla p}{|\nabla p|} = \frac{\vec{V}\cdot\nabla p}{a|\nabla p|} \quad (1)$$

For the ramp roughness, the upstream separation bubble is very small and the separation shock is restricted in a narrow region along the spanwise direction, both the separation and reattaches shocks are convex. For the diamond roughness, the separation shock is the widest due to the largest upstream separation flow (shown in Figure 5), the downstream reattach shock exhibits a concave shape. The shock system for the cylinder is similar with the diamond, except the nearly flat reattach shock. The upstream separation shock and bow shock will join to form a single shock surface at some downstream location.

The vortex structures around and in the wake of the roughness can be visualized utilizing the Q criterion, which is the second invariant of the velocity gradient tensor, given by:

$$Q=\frac{1}{2}\left(|\Omega|^2-|S|^2\right) \quad (2)$$

As shown in Figure 6, a pair of stable vortex tubes is formed near the symmetric plane downstream of the roughness. With increasing the streamwise distance, the strength of the streamwise vortices is large enough, the vortex tube break down to form coherent hairpin vortices, which is characteristic of the transition. Between the hairpin vortices and the flat plate, some small scale streamwise vortices can also be observed. In addition to the vortex streak right behind the roughness, the horseshoe vortices are formed for the diamond and cylinder roughness. From the temperature distribution and Q criterion, it can be found that the horseshoe vortices of the diamond roughness are further away from the mid-plane than the cylinder one, for the ramp obstacle, the horseshoe vortices are much closer to the symmetric plane and difficult to distinguish.

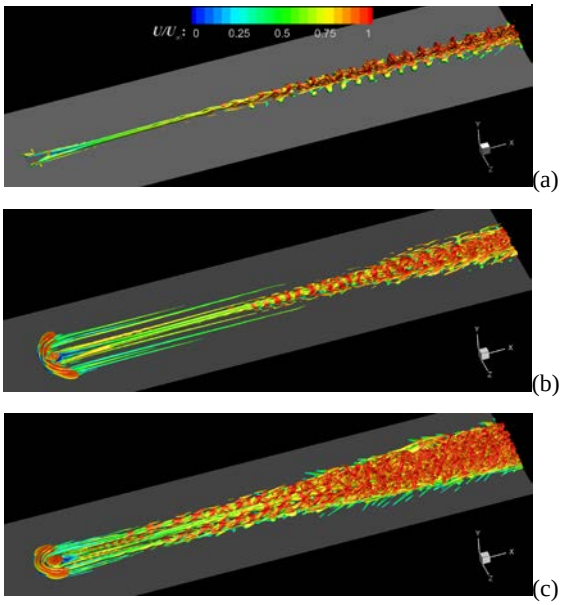

Figure 6. Vortex structure in the wake region
(a) ramp, (b) diamond and (c) cylinder

Effects on Transition

Figure 7 shows the streamwise Reynolds stress distribution on several downstream cross-flow planes, superimposed by contour lines of $u_s = \sqrt{(\partial u/\partial y)^2 + (\partial u/\partial z)^2}$, which can reflect the local shear level. It can be found that u_s distributes around the low-velocity streak, forming three dimensional high shear level streamwise vortices. These 3D shear layers show unstable characteristic, Reynolds stress distributes right around the boundary of shear layers.

For the ramp roughness, instability is constraint in the narrow central region near the roughness (x=10mm), with increasing the streamwise distance (x=40mm), the magnitude of instability grows up, the horseshoe vortices

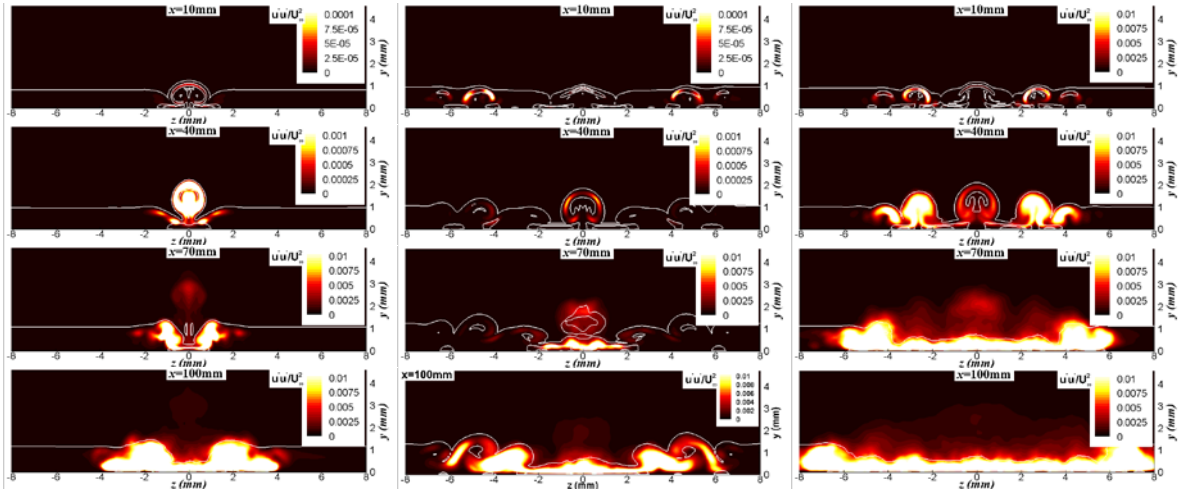

(a) (b) (c)

Figure 7. Streamwise Reynolds stress distribution on the cross sections at four streamwise locations, contour represents the Reynolds stress, white lines represent us. (a) :ramp, (b) diamond, and (c)cylinder

near the flat plane starts to be unstable. At the x=70mm section, the horseshoe vortices are more unstable than the vortex streak near the mid-plane, the instability also travels in the lateral direction along with the wake flow. To the end of the computational domain (x=100mm), the half width of the fully turbulent boundary layer is about 1mm wide. At z>1mm region, the flow is still in the transitional state.

For the diamond and cylinder roughness, the horseshoe vortices are more unstable than the vortex streak that right behind the roughness at the x=10mm section, the flow instability is constraint in the low velocity streak region. With increasing the streamwise distance, for the diamond roughness, the instability generated by the vortices near the mid-plane grows faster, compared with that generated by the horseshoe vortices. For the cylinder roughness, both the wake vortices and the horseshow vortices play an important role in the flow transition. To the end of computation domain (x=100mm) , the half width of the fully turbulent wake of the diamond roughness is about 2.5mm, while it is about 6mm for the cylinder one.

The streamwise variation of the disturbed energy on the symmetric plane is presented in Figure 8, which is defined by $e = \int_{y=0}^{y=\delta} u_i' u_i' / 2 \, dy$. Note that the vertical axis is in the logarithmic scale.

The disturbed energy shows a significant linear growth rate at about x>20mm. The amplitude of disturbed energy is the largest for the cylinder roughness, while its growth rate is the smallest at the range of 20mm<x<50mm. The disturbance of the ramp and the square shows similar growth rate that is larger than the cylinder case during the linear growth range, but the amplitude of the disturbance for the square roughness is the smallest among these three obstacles. The growth of disturbed energy for the ramp slows down at about x=40mm, while it is about x=60mm for the diamond and the cylinder. The saturation is reached at x≈80mm for the ramp roughness, which means the transition occurs, while it is x≈70mm for the square and cylinder case. To the end of the computation domain, the flow reaches the turbulent state, and the amplitudes of the disturbance for the ramp, diamond and cylinder are nearly the same.

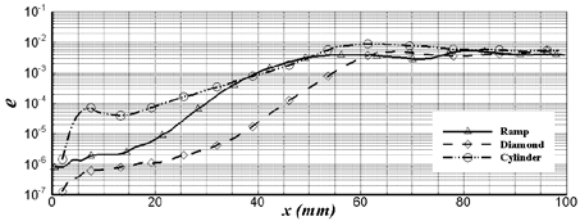

Figure 8. Turbulent kinetic energy evolution in the streamwise direction on the symmetric plane

Effects on Aerothermodynamics and Aerodynamic Performance

The ideal roughness element will trip the flow from laminar to turbulence very rapidly, without producing much drag at the roughness itself and encountering severe thermal environment. In the numerical simulation, not only the transition effects of the three types of roughness are investigated, but also the thermal environment and drag increment caused by the roughness are evaluated.

After the strong bow shock near the head of the roughness, the temperature and pressure increase dramatically, as a result, the roughness will encounter severe thermal environment. The heat flux around the top of the

roughness is very huge, compared with the nearby laminar zone. The value and position of the maximum heat flux that the roughness elements are encountering are shown in Table 3. For the ramp roughness, the maximum heat flux on its top is 16.691 times of the local laminar value. For the diamond and cylinder, the positions of the maximum heat are located at the windward vertex, and their values are 133.691 and 173.793 times of the laminar value, respectively.

Table 3 Maximum non dimensional heat flux ($\times 10^3$) of the roughness elements

	H_{max}	H_{max}/H_{lam}	Position
Ramp	4.106	16.691	Top
Diamond	32.888	133.691	Windward vertex
Cylinder	42.753	173.793	Windward vertex

Table 4 Drag coefficient ($\times 10^4$) for these isolated roughness elements

	C_d (r)	C_d (f)	C_d_p (r)	C_d_v (r)
Ramp	0.124	8.325	0.104	0.020
Diamond	0.640	8.640	0.552	0.089
Cylinder	0.595	9.267	0.489	0.100

The drag force caused by the roughness is also evaluated, as shown in Table 4. The reference area used in the definition of the drag coefficient is the area of the flat plate (5.456×10^{-3} m^2). C_d (r) and C_d (f) represent the drag by the roughness itself and the drag of the flat plate, respectively. C_d_p and C_d_v stand for the pressure drag and the viscosity drag. The drag by the ramp itself is rather small, about 1.468 percent of the total drag, while it's 6.897 and 6.033 percent for the diamond and cylinder roughness, respectively. The drag of the flat plate is totally the viscosity force, affected by the area of the transitional/turbulent wake, so it's the largest for the cylinder and the smallest for the ramp roughness. The viscosity drag force of these three roughness elements is about 20 percent of the pressured drag force.

CONCLUSIONS

In the present study, the hypersonic boundary layer transition induced by three types of isolated roughness element (ramp, diamond and cylinder, respectively) is studied using DNS method. The width of these roughness elements is the same, and their heights are approximately equal to the local undisturbed boundary layer.

The flow transition is dominated by the instability of the counter-rotating streamwise vortices generated by the roughness. For the cylinder, the horseshoe vortices play a more important role than the wake vortices right behind the roughness.

The transition distance downstream of the ramp is about 80mm, a little longer than the diamond and cylinder (70mm), the half width and spreading angle of the transitional/turbulent wake of the ramp are smaller than the other two obstacles, but the growth rate of the disturbance for the ramp is the largest. On the other hand, the maximum heat flux and drag increment caused by the ramp are the smallest among these three roughness elements, while they are largest for the cylinder.

The transition effect, the thermal environment and the drag increment are taken into consideration to compare three roughness elements. Generally, the ramp will be a suitable roughness element in triggering the hypersonic boundary layer transition.

REFERENCES

Bartkowicz, M. D., *Numerical simulations of hypersonic boundary layer transition*, PhD. thesis, University of Minnesota, 2012.

Berry, S.A., Auslender, A.H., Dilley, A.D., and Calleja, J.F., "Hypersonic Boundary-Layer Trip Development for Hyper-X", *Journal of Spacecraft and Rockets*, Vol.38, No.6, Nov.-Dec. 2001, pp.853-864.

Choudhari,M., Li,F., Wu,M., Chang, C.L., Edwards,J., Kegerise,M. and King,R., "Laminar-Turbulent Transition behind Discrete Roughness Elements in a High-Speed Boundary Layer", *AIAA paper 2010-1575*,Jan. 2010.

Duan, Z.W., Xiao, Z.X. and Fu, S., "Direct Numerical Simulation of Hypersonic Transition Induced by an Isolated Cylindrical Roughness Element", *Science China Physics, Mechanics & Astronomy*, Vol. 57, NO.12, Sep. 2014, pp. 2330-2345.

Schneider, S.P, "Effects of Roughness on Hypersonic Boundary-Layer Transition", *Journal of Spacecraft and Rocket*, Vol.45, No. 2, Mar.-April 2008, pp.192-209.

Sterrett, J.R., Morrisette, E. L, Whitehead, A.H., Jr. and Hicks, R.M., "Transition Fixing for Hypersonic Flow", *NASA TND-4129*, Oct. 1967.

Tirtey,S.C., *Characterization of a Transitional Hypersonic Boundary Layer in Wind Tunnel and Flight Conditions*, PhD. Thesis, Von Karman Institute for Fluid Dynamics, Oct. 2008.

Van Driest E.R. and Blumer C.B., "Boundary -Layer at Supersonic Speeds-Three Dimensional Roughness Effects (Spheres)", *Journal of the Aerospace Sciences*, Vol 29, No.8, Aug. 1962.

Van den Dynde,J.P.J.P. and Sandham,N.D., "Numerical Simulation of Roughness Induced Instability Growth and Transition at Mach 6", *AIAA paper 2014-2499*, June 2014.

Wang, Q.J., Ren, Y.X. and Sun, Z.S., "High Resolution Finite Volume Scheme Based on Minimized Dispersion and Controllable Dissipation Reconstruction", *ICCFD7-1004*, July 2012;

Wheaton, B.M., Schneider, S. P., "Instability and transition due to near-critical roughness in a hypersonic laminar boundary layer", *AIAA paper 2013-0084*, Jan. 2013.

Whitehead, A. H., Jr., "Flowfield and Drag Characteristics of Several Boundary-Layer Tripping

Elements in Hypersonic Flow", *NASA, TND-5454*, Oct. 1969.